PHYSICAL REVIEW E **79**, 015401(R) (2009)

Laser-driven inertial ion focusing

H. B. Zhuo,[1,*] Wei Yu,[2,3] M. Y. Yu,[3,4] H. Xu,[1] X. Wang,[2] B. F. Shen,[2] Z. M. Sheng,[5] and J. Zhang[5]
[1]*National Laboratory for Parallel and Distributed Processing, School of Computer Science, National University of Defense Technology, Changsha 410073, China*
[2]*Shanghai Institute of Optics and Fine Mechanics, Chinese Academy of Sciences, Shanghai 201800, China*
[3]*Institute for Fusion Theory and Simulation, Zhejiang University, Hangzhou 310027, China*
[4]*Institute for Theoretical Physics I, Ruhr University, Bochum D-44780, Germany*
[5]*Department of Physics, Jiaotong University, Shanghai 200240, China*
(Received 28 May 2008; published 13 January 2009)

A *Hohlraum*-like configuration is proposed for realizing a simple compact source for neutrons. A laser pulse enters a tiny thin-shelled hollow-sphere target through a small opening and is self-consistently trapped in the cavity. The electrons in the inner shell-wall region are expelled by the light pressure. The resulting space-charge field compresses the local ions into a thin layer that becomes strongly heated. An inward expansion of ions into the shell cavity then occurs, resulting in the formation at the cavity center of a hot spot of ions at high density and temperature, similar to that in inertial electrostatic confinement.

DOI: 10.1103/PhysRevE.79.015401 PACS number(s): 52.38.Kd, 52.58.Qv, 52.50.Lp, 29.25.Dz

With the recent rapid advances in short-pulse laser technology, laser-driven nuclear reaction has become an active area of research [1,2]. The neutron burst produced in such laser-driven reactions can be highly localized and is useful in many applications. Ditmire *et al.* [1] first demonstrated that a fusion reaction can occur when a short laser pulse interacts with deuterium clusters. The atoms are rapidly ionized by the intense laser field, and the freed electrons are expelled by the light pressure. The resulting space-charge field then leads to ion Coulomb explosion, and a fusion reaction can occur when the energetic ions from the clusters collide. The rate of neutron production per unit volume per unit time is given by [2] $P=n_i^2\langle\sigma v\rangle$, where n_i is the density of the ions and $\langle\sigma v\rangle$ is the Maxwellian-averaged reactivity, which reaches a maximum at the temperature $T_i=1.25$ MeV for DD reaction and $T_i=64$ keV for the DT reaction. Thus, to obtain more neutrons, the ion density should be as high as possible and the ion temperature should be such that the reactivity is maximized for fusion reaction [1]. It follows that a key issue of the laser-driven neutron source is the proper target configuration that can lead to a high concentration of plasma ions at the appropriate temperature.

In this paper, we propose a target configuration suitable for neutron production. The target is a dense spherical shell, similar to that used in *Hohlraum* inertial-confinement fusion, except that its size is only a few laser wavelengths. When an intense short laser pulse is sent into the shell cavity through an opening, the radiation field self-consistently fills the entire shell cavity. The trapped laser behaves like a spherical light pulse and ionizes the inner shell surface, and the radiation pressure drives the local electrons radially outward. The resulting space-charge field accelerates the local ions into the dense target, forming a shocklike highly compressed layer [3,4]. The latter becomes strongly heated and the thermal pressure can lead to inward plasma expansion. Because of the symmetry, on average the inward-moving ions are ballistically focused at the cavity center. As a result, a peak of high ion density and temperature is produced, providing a favorable condition for the fusion reaction.

We use a two-dimensional particle-in-cell code to simulate the interaction of a high-power laser pulse with a shell target. In the simulation, the shell is approximated by an infinitely long hollow cylinder with inner radius $4\lambda_0$ and outer radius $6\lambda_0$, where λ_0 is the laser wavelength. The shell cavity center is at $y=15\lambda_0$ and $z=10\lambda_0$. The shell plasma is of density $4n_c$, where n_c is the critical density. A *p*-polarized laser pulse with strength parameter $a=5$ and spot radius $2\lambda_0$ is sent along the z axis into the shell interior through a 40° opening. The pulse has a sine profile and its duration is $20T_0$, where T_0 is the laser period. The computation box is $30\lambda_0 \times 30\lambda_0$ and has a spatial resolution up to 100 cells per wavelength, with each cell containing 200 ions and 200 electrons. The electron-ion mass ratio is 1/1836, and the initial temperature of the Maxwellian electrons and ions is 1 keV. The computation box is periodic in the transverse direction and absorbing at the right end.

At $t=50T_0$ most (about 70%) of the laser pulse has entered and filled the cavity, with the remaining laser light

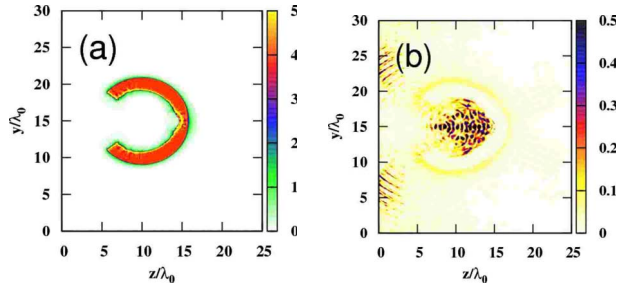

FIG. 1. (Color online) Distributions of ion density (a) and electromagnetic energy density (b) at $t=50T_0$. The ion density is normalized by n_c, the electromagnetic energy density by $m_e c^2 n_c \Delta^2$, where Δ is the grid spacing, T_0 the laser period, $L=20T_0$ the pulse duration, $w=2\lambda_0$ the spot radius, and $a=5$ the laser strength parameter. The initial shell-target density is $n=4n_c$. The inner radius of the shell is $4\lambda_0$ and outer radius $6\lambda_0$.

*Corresponding author. zhb_pic_2d@sina.com

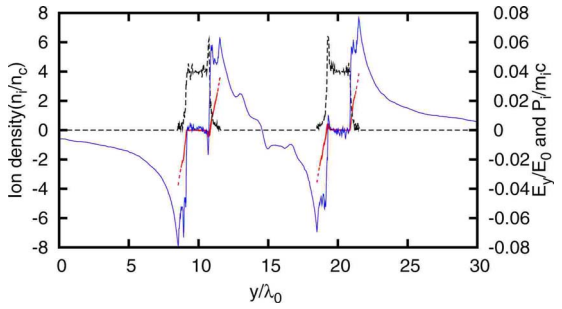

FIG. 2. (Color online) Ion density (black dashed line), momentum (red points), and electric field (blue solid line) distributions at $z=10\lambda_0$ (a plane through the cavity center) and $t=50T_0$.

reflected or scattered backward. Some of the inner-surface electrons have been driven out into the cavity as well as into the outer vacuum region, forming an electron sheath and a space-charge field around the entire target surface. The space-charge field drives out some of the surface ions by target-normal surface acceleration (TNSA) [5] to form a thin low-density ion sheath around the target surface, as can be seen in Fig. 1. Figure 1(b) shows the electromagnetic energy distribution. One can see that the laser field is self-consistently trapped in the cavity as in a resonant-cavity mode. The trapped light remains nearly coherent and intense. It will thus continue to exert pressure on the cavity-wall plasma until it is completely dissipated. A fraction (about 30% in the entire laser-plasma interaction process) of the laser energy is reflected and scattered through the cavity entrance. The low-field and energy region adjacent to the outer shell surface can be attributed to the space-charge field produced by the laser-evacuated target electrons, as can also be seen in Fig. 2 for the electric field, ion density, and ion momentum at $z=10\lambda_0$ and the same time. The space-charge field inside the cavity, also due to the laser-expelled electrons, acts like a potential well for ions. In Fig. 2 one can also see the TNSA ion motion and the resulting ion sheaths outside the inner as well as outer shell surfaces, as expected [5]. The corresponding electron sheaths (not shown) due to the ponderomotively expelled electrons are a few times thicker. Finally, Figs. 1(a) and 2 also show that the ions in the inner shell surface are being compressed by the local space-charge field into a high-density shocklike layer, since they cannot freely move through the dense target interior like the electrons. The maximum ion density in the compressed layer is more than $5n_c$ at this instant.

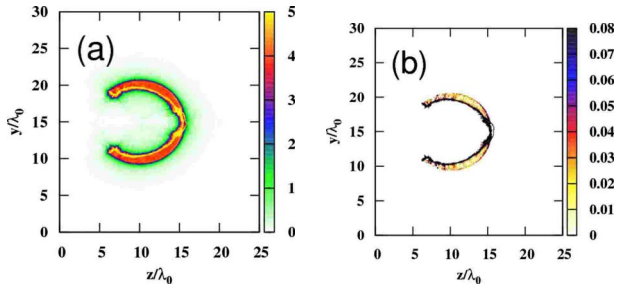

FIG. 3. (Color online) Distributions of the ion density n_i (a) and the ion temperature (b) at $t=100T_0$. The ion density n_i is normalized by n_c and the ion temperature T_i is in MeV.

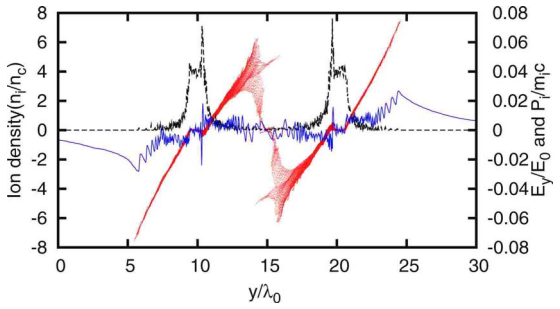

FIG. 4. (Color online) Ion density (black dashed line), momentum (red points), and electric field (blue solid line) distributions at $z=10\lambda_0$ and $t=100T_0$.

Figure 3(a) shows the ion density and Fig. 3(b) the ion thermal pressure at $t=100T_0$, when the light pressure has effectively vanished. The electrons in the target can now redistribute to partially neutralize the ion-rich regions, and the charge-separation field there becomes significantly weakened, as can be seen in Fig. 4. In Figs. 3(a) and 4 we see that the density in the thin compressed ion layer (now partly neutralized and moved slightly into the dense target) reaches almost $8n_c$. In fact, it turns out that this compressed plasma layer can survive for a long time after the light field has vanished, with its peak density remaining larger than $4n_c$ until about $t=250T_0$. The plasma in the compressed layer is strongly heated, creating a sharp peak in the ion thermal pressure $p_i=n_iT_i$, where T_i is the ion temperature, as can be seen in Fig. 3(b). This high-pressure plasma layer can lead to thermal plasma expansion. The inner and outer electron sheaths (not shown) are now several times the shell thickness, so that the entire cavity is uniformly filled with electrons. Within the shell target and the compressed layer the ion density is about $1n_c$ higher than the electron density, and the overall target profile still remains unchanged. Figure 3(a) shows that inside the cavity there appears to be ions streaming toward the cavity center. From the ion momentum and electric field profiles in Fig. 4, these ions can be recognized as TNSA ions. Similar perpendicular-to-surface streaming ions can also be seen at the cavity entrance wall. As the ions start to fill the cavity, the space-charge field (and thus the depth of the corresponding potential well) is reduced, as can be seen in Fig. 4. However, the ions continue to stream radially into the cavity since the pressure of the compressed layer remains high. The apparent complex ion momentum distribution near the cavity center can be attributed to the

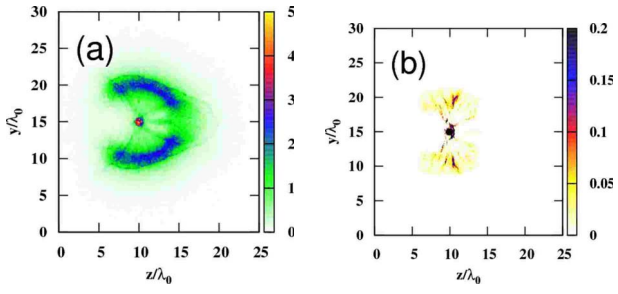

FIG. 5. (Color online) Distributions of ion density (a) and temperature (b) at $t=300T_0$.

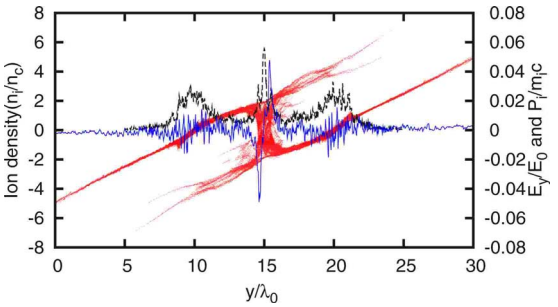

FIG. 6. (Color online) Ion density (black dashed line), momentum (red points), and electric field (blue solid line) distributions at $z=10\lambda_0$ and $t=300T_0$.

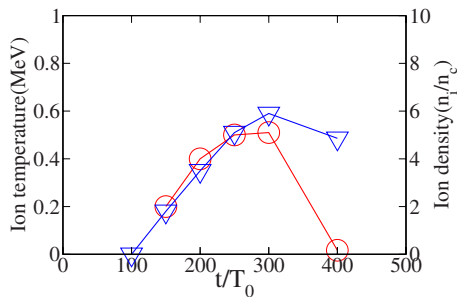

FIG. 7. (Color online) Time evolution of the ion density (blue triangles) and temperature (red circles) at the cavity center.

geometrical effect that there the ions can easily enter and leave the $z=10\lambda_0$ plane as they are deflected by the (now strongly fluctuating) field of the trapping potential.

The compressed plasma layer continues to move radially outward and it eventually becomes merged with the shell plasma. The peak of the merged plasma inside the shell body remains at about $8n_c$ until $t=250T_0$. Simultaneously, ions from the compressed layer continue to be driven into the cavity by the space-charge field and the thermal pressure. The ions slow down and aggregate at the center, and a positive potential peak is built up which reflects and deflects the ions that are still coming it. As the ions slow down and/or change direction, their streaming energy is converted into thermal energy, as shown in Fig. 5 for the ion density and temperature distributions $t=300T_0$ as well as in Fig. 6 for the corresponding electric field, ion density, and momentum at $z=10\lambda_0$. This process continues until the ion density and temperature of the highly localized hot spot at the cavity center reach maximum, namely, $\sim 6n_c$ and ~ 0.6 MeV, respectively, as shown in Fig. 7 for the evolution of the ion density and temperature at the cavity center. Thus, the density is sufficiently high and the temperature appropriate for the fusion reaction to occur. The spatial distribution (not shown) of the nearly Maxwellian electrons is similar to that of the ions, except that the electron density inside the cavity and the shell remains lower, so that the hot spot is accompanied by a positive space-charge field. The low-density electron sheath surrounding the shell remains much thicker than that of the ion. With the loss of particles from the shell plasma, the ion density in the original shell region is reduced to about $2n_c$, i.e., half the initial density. Except within the hot spot at the center of the cavity, the ion pressure is everywhere negligibly small. One can also see in Fig. 7 that the hot spot already begins to appear at $t=100T_0$. After $t=300T_0$, the particles in the hot spot begin to spread radially outward due to the high thermal pressure there, and the density and temperature at the center decrease rapidly.

In conclusion, we have shown that a tiny spherical shell can be a suitable target configuration for a compact laser-driven neutron source. The present approach is somewhat similar to the *Hohlraum* approach in inertial confinement fusion, although the physics involved is quite different. Here we have made use of the recent understanding of the interaction of intense short-pulse lasers with thin curved targets [5–7]. In particular, Patel *et al.* [6] experimentally verified TNSA proton focusing by a hemispherical target back side, and Okada *et al.* [7] showed that a parabolic target back side is best for proton focusing. The present scheme differs from the well-studied curved targets in that here the *Hohlraum* involved is much smaller, such that the shell cavity allows a short laser pulse to be trapped self-consistently like a cavity mode. As a result, much more efficient and longer interaction with the shell plasma can take place, and ions can be ballistically focused to the cavity center to form a dense hot spot. The approach here is also similar to that of ion focusing in inertial electrostatic confinement (IEC) [8–12], where ions in a spherical container (acting as the anode) are accelerated electrostatically by a spherical wire grid (acting as the cathode) inside it. As in IEC, in our scheme the ions are ballistically focused toward the center of the cavity to form a hot spot favorable for neutron production [8,10–12]. In the IEC experiments, a highly localized ion peak and electrostatic potential structure similar to those in Fig. 4 have been observed. To a lesser extent our scheme also resembles the *Z*-pinch [13], the plasma focus [14], and some ion-beam devices [15], where the plasma is electromagnetically pinched to the center. However, in these schemes a spot of either high temperature or high density, but not both, is produced [13–15].

This work was supported by the National High-Tech ICF Committee of China, the Natural Science Foundation of China under Grants No. 10505030, No. 10505031, No. 10676010, No. 10474081, No. 10576035, No. 10675024, No. 10775165, No. 10335020, No. 10575013, No. 10576007, and No. 10835003, the National Basic Research Program of China (973 Program) under Grants No. 2007CB815101 and No. 2006CB806004, and the Japan-Korea-China cooperation on "High Energy Density Sciences for Laser Fusion Energy."

[1] T. Ditmire *et al.*, Nature (London) **398**, 489 (1999).
[2] S. Atzeni and J. Meyer-ter-Vehn, *The Physics of Inertial Fusion* (Oxford University Press, Oxford, 2004).
[3] J. Denavit, Phys. Rev. Lett. **69**, 3052 (1992).
[4] B. F. Shen *et al.*, Phys. Rev. E **71**, 015401(R) (2005).
[5] S. C. Wilks *et al.*, Phys. Plasmas **8**, 542 (2001).
[6] P. K. Patel *et al.*, Phys. Rev. Lett. **91**, 125004 (2003).
[7] T. Okada, A. A. Andreev, Y. Mikado, and K. Okubo, Phys. Rev. E **74**, 026401 (2006).
[8] R. Hirsch, J. Appl. Phys. **38**, 4522 (1967).
[9] T. H. Rider, Phys. Plasmas **2**, 1853 (1995).
[10] T. A. Thorson *et al.*, Phys. Plasmas **4**, 4 (1997).
[11] R. P. Ashley *et al.*, Fusion Technol. **39**, 546 (2001).
[12] K. Yoshikawa *et al.*, Nucl. Fusion **41**, 717 (2001).
[13] D. D. Ryutov *et al.*, Rev. Mod. Phys. **72**, 167 (2000).
[14] V. A. Gribkov *et al.*, J. Phys. D **40**, 3592 (2007).
[15] H. Hora *et al.*, Proc. SPIE **5627**, 51 (2004).